REPORT DOCUMENTATION PAGE

Form Approved
OMB No. 0704-0188

1. REPORT DATE *(DD-MM-YYYY)*	2. REPORT TYPE	3. DATES COVERED *(From - To)*
01-07-2010	Technical Paper	

4. TITLE AND SUBTITLE

A Preliminary Study of Krypton Laser-Induced Fluorescence

5a. CONTRACT NUMBER

5b. GRANT NUMBER

5c. PROGRAM ELEMENT NUMBER

6. AUTHOR(S)
William A. Hargus, Jr. (AFRL/RZSS)

5d. PROJECT NUMBER

5e. TASK NUMBER

5f. WORK UNIT NUMBER
23080535

7. PERFORMING ORGANIZATION NAME(S) AND ADDRESS(ES)

Air Force Research Laboratory (AFMC)
AFRL/RZSS
1 Ara Road
Edwards AFB CA 93524-7013

8. PERFORMING ORGANIZATION REPORT NUMBER

AFRL-RZ-ED-TP-2010-312

9. SPONSORING / MONITORING AGENCY NAME(S) AND ADDRESS(ES)

Air Force Research Laboratory (AFMC)
AFRL/RZS
5 Pollux Drive
Edwards AFB CA 93524-7048

10. SPONSOR/MONITOR'S ACRONYM(S)

11. SPONSOR/MONITOR'S NUMBER(S)
AFRL-RZ-ED-TP-2010-312

12. DISTRIBUTION / AVAILABILITY STATEMENT

Approved for public release; distribution unlimited (PA #10384).

13. SUPPLEMENTARY NOTES
For presentation at the 46th AIAA/SME/SAE/ASEE Joint Propulsion Conference, Nashville, TN, 25-28 July 2010.

14. ABSTRACT

There is growing interest in the use of krypton as propellant for electric propulsion as a lower cost replacement for xenon. This study examines the potential applications of laser-induced fluorescence as a plasma diagnostic technique for Kr I and Kr II. Candidate electronic transitions are examined to determine their suitability for successful routine application of laser-induced fluorescence. Criteria considered include lower state populations, optical accessibility, existence of nonresonant fluorescence transitions, and fluorescence branching ratios. Using these criteria, one transition for each Kr 1 and Kr II are identified for future development.

15. SUBJECT TERMS

16. SECURITY CLASSIFICATION OF:			17. LIMITATION OF ABSTRACT	18. NUMBER OF PAGES	19a. NAME OF RESPONSIBLE PERSON
					Dr. William A. Hargus, Jr.
a. REPORT	b. ABSTRACT	c. THIS PAGE			19b. TELEPHONE NUMBER *(include area code)*
Unclassified	**Unclassified**	**Unclassified**	SAR	12	N/A

A Preliminary Study of Krypton Laser-Induced Fluorescence

William A. Hargus, Jr.*
Air Force Research Laboratory, Edwards Air Force Base, CA 93524

There is growing interest in the use of krypton as propellant for electric propulsion as a lower cost replacement for xenon. This study examines the potential application of laser-induced fluorescence as a plasma diagnostic technique for Kr I and Kr II. Candidate electronic transitions are examined to determine their suitability for successful routine application of laser-induced fluorescence. Criteria considered include lower state populations, optical accessibility, existence of nonresonant fluorescence transitions, and fluorescence branching ratios. Using these criteria, one transition for each Kr I and Kr II are identified for future development.

Introduction

THIS study investigates potential electronic transitions for laser-induced fluorescence of krypton neutrals (Kr I) and singly ionized ions (Kr II). A number of selection criteria will be used to determine preferred electronic transitions. These include the identification of highly populated states suitable for excitation, resonant and non-resonant fluorescence collection schemes, fluorescence branching ratios, and the availability of isotopic and hyperfine structure data so that the transitions can be suitably modeled.

At present, xenon (Xe) is the propellant of choice for most electrostatic plasma thrusters including Hall effect thrusters. The selection of xenon is due to a number of engineering reasons. These include the high mass (131 amu) and relatively low ionization potential (12.1 eV) of xenon; as well as inert nature of xenon which eliminates much of the controversy that plagued early electrostatic propulsion efforts when mercury (Hg) and cesium (Cs) were the propellants of choice.[1] Although xenon is a noble gas, it is the heaviest, and due to its non-ideal gas behavior, it is possible to pressurize and store with room temperature specific densities exceeding unity.[2,3] As such, it actually can be stored at slightly higher densities than that of the common liquid monopropellant hydrazine.

While xenon will likely remain the ideal propellant for electrostatic electric propulsion thrusters such as Hall effect thrusters, there are several concerns that have driven the Hall effect thruster community to explore alternative propellants. As orbit raising missions of longer duration and larger payloads are proposed for Hall effect thrusters, the mass of required propellant increases. Xenon production is presently a byproduct of the fractional distillation of atmospheric gases for use primarily by the steel industry. Due to the low concentration of xenon in the atmosphere (∼90 ppb), worldwide production appears to be limited to approximately 6000 standard cubic meters per year. Increasing industrial demand for items such as high efficiency lighting and windows as well as plasma based micro–fabrication has produced wide price swings in the past decade. Xenon prices have varied by as much as factor of ten in the past three years alone.

For missions that can benefit from higher specific impulse, krypton will have benefits beyond its lower cost. Krypton has a lower atomic mass (83.8 amu),but a slightly higher ionization potential (14.0 eV) than xenon. Like xenon, krypton is a noble gas and could be easily integrated into existing xenon propellant management systems without much modification. The similar ionization potential would likely not dramatically affect the efficiency of a Hall effect thruster and the lower mass would produce a 25% increase in specific impulse. The increase in specific impulse would be useful for missions such as station-keeping where increased specific impulse is an advantage. For missions such as orbit raising, increasing the specific impulse would increase trip time due to power limitations. However as solar electric power system specific power decreases, increasing the specific impulse of the propulsion system is advantageous. Krypton is approximately 10x more common in the atmosphere (and hence in production) than xenon, and when accounting for mass is approximately 6x less expensive. Table 1 summarizes the properties of xenon and krypton.[2]

Laser-Induced Fluorescence

Laser-induced fluorescence (LIF) may be used to detect velocity-induced shifts in the spectral absorption of various plasma species. The fluorescence is monitored as a continuous-wave laser is tuned in frequency over the transition of interest, of energy $h\nu_{12}$, where h is Plank's constant, ν_{12} is wavenumber of transition between lower state 1 and higher energy state 2. Note that state 1 may be the ground state, but any sufficiently highly populated excited state will do.

*Senior Aerospace Engineer, AFRL/RZSS, Edwards AFB, Associate Fellow AIAA.

Table 1 Comparison of xenon and krypton properties critical for electrostatic propulsion.[2]

Property	Units	Xe	Kr
Atomic Mass	amu	131.3	83.8
1^{st} Ionization Energy	eV	12.1	14.0
2^{nd} Ionization Energy	eV	21	24
3^{rd} Ionization Energy	eV	32	37
Atmospheric Concentration	ppb	87	1000
Stable Isotopes		9	6
Odd Isotopes		2	1
Critical Pressure	MPa	5.84	5.50
Critical Temperature	K	290	209
Boiling Point (1 atm)	K	161	120

Measurements can be made with high spatial resolution, determined by the intersection of the probe laser beam with the fluorescence optical collection volume.

Velocity measurements can be made using laser-induced fluorescence velocimetry as an atom, or ion, moving with a velocity component u relative to the direction of the incoming laser will absorb the light at a frequency shifted from that of stationary absorbers due to the Doppler effect. The magnitude of this frequency shift $\delta\nu_{12}$ is

$$\delta\nu_{12} = \frac{u}{c}\nu_{12} \tag{1}$$

The measured fluorescence signal is given by:[4,5]

$$S_f = \eta_d \alpha_c h \nu_{12} A_{21} N_2 \tag{2}$$

where η_d is the efficiency of the detection system, α_c accounts for geometric factors involving the collection system, and A_{21} is the Einstein coefficient for spontaneous emission of the relevant transition. For low laser intensities, rate equation analysis indicates that the upper level population N_2, and therefore the fluorescence signal, is linearly dependent on laser intensity at steady state, i.e.

$$N_2 \sim I_\nu B_{12} \phi_\nu \tag{3}$$

where I_ν is the spectral irradiance at frequency ν, B_{12} is the Einstein stimulated absorption coefficient, and ϕ_ν is the transitions spectral line shape which accounts for the variation of the absorption or laser excitation with frequency. The line shape is determined by the environment of the absorbing atoms, so an accurate measurement of the line shape function can lead to the determination of a number of plasma parameters. The variation of the resultant velocities has been found found, in various studies, to be less than the experimental uncertainty for the ions (±500 m/s), or for the neutrals (±60 m/s).[6–8]

Several factors affect the line shape and give rise to broadening and/or a shift of the spectral line. In high-temperature plasmas, the most significant is Doppler broadening due to the absorber's random thermal motion, characterized by the atomic, or ionic, kinetic temperature, T_{kin}. When the absorbing species velocity distribution is Maxwellian in shape, the Doppler broadening results in a Gaussian line shape. Collisional interactions between the absorbers and other species in the plasma give rise to spectral line shapes that are often Lorentzian. This includes interactions with charged particles (Stark broadening) and uncharged particles (van der Waals broadening). If both Doppler broadening and collisional broadening are important and independent, the resulting line shape is a convolution of the Gaussian and Lorentzian line shape into a Voigt line shape.[5]

The absorption line shape is an intrinsic property of the absorbers, whereas the fluorescence excitation line shape is the variation in the detected fluorescence signal with frequency as the laser is tuned across the absorption line feature. If the laser excitation significantly perturbs the populations of the coupled levels, it is said to be saturating the transition and the fluorescence signal is then a nonlinear function of laser intensity. In cases where the laser intensity is significantly below the saturation level and the laser line width is small compared to the measured line width, the fluorescence excitation line shape reflects the spectral absorption line shape as given by Eqn. 2 and Eqn. 3. When the laser intensity is sufficiently high to saturate the transition, the fluorescence excitation line shape is broader than the spectral line shape and the fluorescence intensity is less than it would be if it were linear with the laser intensity I_ν. The saturation intensity, defined as that intensity which produces a fluorescence signal half of what it would be if the fluorescence was linear with I_ν, depends inversely on the line strength of the particular transition. Stronger transitions have a smaller saturation intensity and thus a larger saturation effect for a given laser intensity.[5]

LIF is a convenient diagnostic for the investigation of ion and atomic velocities as it does not physically perturb the plasma. The LIF signal is a convolution of the velocity distribution function (VDF), transition line shape, and laser beam frequency profile. Determination of the VDF from LIF data only requires the deconvolution of the transition line shape and laser beam profile from the raw LIF signal trace. Alternatively, the line shape itself can also provide valuable information on the state of the plasma, such as electron density, pressure, or heavy species temperature. In the somewhat turbulent plasmas typical of Hall effect thrusters, the fluoresce line shape can also be indicative of the relative motion of the ionization zone as it axially traverses.[9,10] However, care must be taken to ensure that the relative effects of these phenomena are separable. In addition, magnetic (Zeeman effect) and electric (Stark effect) fields can also influence the fluorescence line shape[11] and must be accounted for when

analyzing the line shapes should the fields be of sufficient magnitude. In the case of LIF of ions in a Hall effect thruster, the fluorescence line shape appears to be most indicative of the aforementioned plasma turbulence including periodicity in the positions of the ionization zone within the acceleration channel.

Usage

Over the past 20 years, plasma based propulsion technology has advanced from an academic curiosity to an accepted engineering practice. This is most keenly felt in the geosynchronous orbit (GEO) communications satellite industry where the use of electric propulsion represents a significant fraction of spacecraft north-south station keeping propulsion. The use of electric propulsion reduces propellant mass by an order of magnitude and simultaneously increases payload, and hence revenue, significantly.

Still, there has been a reluctance to embrace plasma propulsion by the spacecraft community. Not simply due to conservative spacecraft design practices, but stemming from the recognition that highly the accelerated plasma plume ions have the potential to severely impact the performance of mission critical instruments. As spacecraft power increases, plasma propulsion will continue to gain advantages due to increased thrust levels and its inherently high specific impulse. Yet, valid integration concerns will grow in severity with increased power transferred to these highly accelerated plasma plumes.

LIF provides a convenient measure of the plasma acceleration both within and in the near plume of a plasma thruster. Ultimately, these plasma sources, today most commonly electrostatic thrusters such as *ion engines* and *Hall effect thrusters*, use electric fields to accelerate their ionized propellant to very high velocities, sometimes in excess of 20 km/s over spatial dimensions of on order of 1 cm. As a result, LIF provides a unique capability to measure these velocities and their spatial rate of change nonintrusively, without impact to the plasma. This measurement capability is critical in understanding the yet poorly modeled distribution of electric potential, *vis–a–vi* the electric field, particularly of Hall effect thrusters. Furthermore, since the fluorescence line shape here is ultimately a convolution of the transition lineshape and the species velocity distribution function (VDF), it is possible without too much difficulty to extract a time averaged VDF using knowledge of the transition lineshape. Finally, it is important to note that comparison of VDF data derived from numerical models and LIF measurements is one of the more fundamental comparisons of the two archetypes.

In addition to the need to understand the acceleration of the ionized propellant, the velocity field of the neutral propellant is of value. As an example, Hall thrusters produce thrust by the acceleration of ions through an electric field. Xenon ions will exit Hall thrusters at ∼15 km/s. However, approximately 10% of the propellant flow is not ionized and escapes the acceleration channel at thermal velocities (100–300 m/s). The densities of these two populations is nearly equal due to the wide difference in velocities. These high neutral densities influence electron transport by providing collision partners for low energy electrons seeking to cross magnetic field lines. Neutrals are also a source of charge exchange collision partners with the ion stream. Charge exchange may be responsible for the creation of highly divergent low–energy ions which influence Hall thruster spacecraft integration. In addition, how neutrals flowing though the thruster interact with the background neutrals in ground test facilities is a growing concern. Understanding the differences between ground test and on–orbit thruster operation is an emerging area of study.

To date, the only Hall effect thruster LIF measurements have been on xenon[6,8,12–14] . Several transitions have been examined for both neutral and singly ionized xenon. There is growing literature on the subject of xenon LIF within Hall effect thrusters. With the exception of one conceptual examination of krypton ion spectroscopy,[15] krypton laser spectroscopy has not received any study in the plasma propulsion community. As krypton appears to be a possible propellant replacement candidate for xenon, the goal of this paper is to explore the possibility of applying some of the lessons previously learned for xenon to the development of LIF for krypton Hall effect and other thrusters.

Transition Selection

Selecting a transition for LIF in low density plasma such as that in the near–field of a Hall effect thruster is constrained by a number of factors. First, is the transition laser accessible and are suitable lasers available? Second, does the energy level being probed have a sufficient population to produce substantial signal? There are a number of related issues, but these two are those that define the problem.

Tunable lasers are available in three types that have been applied to plasma LIF. Dye lasers were the traditional source of tunable lasers for plasma and combustion work. These lasers remain workhorses, but suffer from complex user interactions due to the use of liquid lasing medium with finite lifetime. Titanium sapphire (Ti:Sapphire) and alexandrite lasers have similar system complexity, but use a solid state material as the lasing medium. Both these types of lasers can be challenging to work with, but often provide unique capabilities especially with regard to wavelength range and power outputs. The more recent arrival on the scene is the tunable diode laser. These lasers are generally limited to the red and near IR, but there are some limited semiconductor band gaps producing systems in the blue and near ultraviolet (UV). Despite their rel-

atively low power (usually <100 mW and more often <10 mW), these laser systems have been repeatedly demonstrated to be able to produce nearly turnkey LIF systems. In addition, tunable diode laser systems are 10 to 100 times less expensive than the more capable, but much more difficult to maintain tunable dye laser systems.

Since working in the vacuum UV is difficult, the ground state is not likely to be accessed. This requires that the LIF measurements use other states with high populations. Since the densities of Hall effect plasmas is seldom higher than 10^{18} m^3, collisional de-excitation of excited states is a slow process. Therefore, metastable states, which have no allowed radiative decay path, are usually highly populated. Once identified, these states can be used as suitable lower states for laser probing. It should be noted that non-metastable states can be used for LIF in these plasmas; however, their use significantly reduces signal strength and extends the integration time for successful signal recovery.[16]

Krypton Spectroscopy

While a significant amount of spectroscopic study has been performed on various neutral xenon metastable states for atomic clock use, the studies of neutral krypton (and to some extent Kr II as well) have focused on nuclear detection. For example, ^{85}Kr is a uranium and plutonium fission product with a half life of 10.76 years. Due to weapon testing, ^{85}Kr has an occurrence 30% higher in the upper latitudes of the northern hemisphere when compared to the upper latitudes of the southern hemisphere.[17]

Of the 31 known isotopes of Kr, only six have atmospheric concentrations greater than 0.3%. Of these six isotopes between 78 amu and 86 amu, only one, ^{83}Kr has an odd number of neutrons (recall that krypton's atomic number is 36).[2] This is important in the high resolution analysis of atomic spectra since each will have a slight difference in their electron transition energies due to their differences in nuclear mass. This effect has been described in detail previously for xenon in the development of Hall thruster laser diagnostics[6,12]

Table 2 Naturally Occurring Krypton Isotope Properties.[2,18]

Mass (amu)	Abundance	Nuclear Spin
78	0.35%	0
80	2.27%	0
82	11.56%	0
83	11.55%	$\frac{9}{2}$
84	56.90%	0
86	17.37%	0

The odd mass isotopes are further spin split due to nuclear magnetic dipole and electric quadrapole moments. Nuclei which have an odd number of protons and/or an odd number of neutrons possess an intrinsic nuclear spin $\mathbf{I}h/2\pi$, where $\mathbf{I}$ is integral or half-integral depending on if the atomic mass is even or odd, respectively[19] and boldface is used to denote vector quantities. For nuclei with non–zero nuclear spin (angular momentum, $\mathbf{J}$), the interaction of the nucleus with the bound electrons lead to the splitting of levels with $\mathbf{J}$ into a number of components, each corresponding to a specific value of the total angular momentum $\mathbf{F} = \mathbf{I} + \mathbf{J}$.[20] As a result of this interaction, $\mathbf{F}$ is a conserved quantity while $\mathbf{I}$ and $\mathbf{J}$ individually are not. The interaction is weak, allowing the hyperfine splitting of each level to be taken independently of the other levels. The number of nuclear spin split hyperfine components is $2I + 1$ if $J \geq 1$ and $2J + 1$ if $J < 1$, with F taking on the values $F = J + I, J + I - 1, ..., |J - I|$ [12, 13] while satisfying the selection rules imposed on F, i.e. $\Delta F = 0, \pm 1$, unless $F = 0$, in which case $\Delta F \neq 0$.

With these selection rules on the quantum numbers for a particular electronic transition, and with knowledge of the hyperfine structure constants which characterize the magnetic dipole and electric quadrupole moments of the nucleus,[19] the hyperfine energy shifts from the position of the energy for the unshifted level with angular momentum J can be easily calculated.[21]

Two constants are associated with the magnitude of hyperfine nuclear spin splitting.[19] These are the A hyperfine structure constant which represents the nuclear magnetic dipole effect on the atom, and the B hyperfine structure constant which is associated with the nuclear electric quadrapole moment of the atom which will only be present if $I \leq 1$. The relative energy of the spin split states depends on the sign of A . In atoms with $A > 0$, the state with the highest value of F has the highest energy. While for atoms with $A < 0$, the state with the lowest value of F has the highest energy.[21] The energy level shift ΔE_M associated with the magnetic dipole of the nucleus is given by Cowan.[19]

$$\Delta E_M(F) = \frac{1}{2}A[F(F+1)J(J+1)I(I+1)] = \frac{A}{2}C \quad (4)$$

Additionally, the energy spacing between successive levels $F - 1$ and F may be shown to be proportional to F.

$$\Delta E_M(F) - \Delta E_M(F-1) = AF \quad (5)$$

If $I \geq 1$, the nucleus will have an electric quadrapole moment and a related hyperfine splitting constant B which produces an additional hyperfine splitting with energy linear in $C(C+1)$ where C is previously defined in Eqn. 4.

$$\Delta E_F = \Delta E_M + \Delta E_Q \quad (6)$$

$$\Delta E_F = \frac{AC}{2} + \frac{B[\frac{3}{2}C(C+1)2I(I+1)J(J+1)]}{4I(2I-1)J(2J-1)} \quad (7)$$

Where ΔE_F is the combined nuclear spin split energy level shift combining the effect from the nuclear magnetic dipole moment ΔE_M and the effect of the electric quadrapole moment ΔE_Q.[19] It should be noted that the center of gravity of the hyperfine levels lies at a position of the unsplit level J.[20]

$$\sum_F (2F+1)\Delta E_F \quad (8)$$

Due to close energy spacing of nuclear spin split levels, near ideal coupling between **I** and **J** occurs in most hyperfine structure. Therefore, the intensity S rules derived by White for Russel–Saunders coupling are appropriate for hyperfine splitting.[21]

For $J-1 \rightarrow J$,

$F-1 \rightarrow F$:

$$S = \kappa \frac{(Q+I+1)(Q+I)(Q-I)(Q-I-1)}{F} \quad (9)$$

$F \rightarrow F$:

$$S = -\kappa \frac{(Q+I+1)(Q-I)(W+I)(W-I-1)(2F+1)}{F(F+1)} \quad (10)$$

$F+1 \rightarrow F$:

$$S = \kappa \frac{(W+I)(W+I-1)(W-I-1)(W-I-2)}{F+1} \quad (11)$$

For $J \rightarrow J$,

$F-1 \rightarrow F$:

$$S = -\kappa \frac{(Q+I+1)(Q-I)(W+I+1)(W-I)}{F} \quad (12)$$

$F \rightarrow F$:

$$S = \kappa \frac{[J(J+1)+F(F+1)+I(I+1)]^2(2F+1)}{F(F+1)} \quad (13)$$

$F+1 \rightarrow F$:

$$S = -\kappa \frac{(Q+I+2)(Q-I+1)(W+I)(W-I-1)}{(F+1)} \quad (14)$$

Where S is the transition strength and κ is an arbitrary constant. The variables $Q = J + F$ and $W = J - F$ are only introduced to compress the notation.

The relative intensities of the isotope shifted transitions are proportional to each isotope's relative abundance. However, the relative intensities of the nuclear spin split hyperfine splitting are governed by two summation rules.[20] First, the sum of the intensities of all the lines of the hyperfine structure of a transition $J \rightarrow J'$ originating from a component F of the level J is proportional to the statistical weight of this component, $(2F+1)$. Second, the sum of the intensities of all the lines of the hyperfine structure the transition $J \rightarrow J'$ ending on the component F' of the level J' is proportional to the statistical weight of this component, $(2F'+1)$. With these two sum rules, a system of linear equations are solved for the relative intensities of the nuclear spin split components of each isotope.

The practical issues associated with hyperfine isotopic spin splitting in the measurements of plasma acceleration in the plume and within Hall effect thrusters are that the even isotopes broaden the line width to some degree, while the odd isotopes may create much more complex transition structure in high resolution. To some extent hyperfine spin splitting can be neglected for some transitions. For example, the $5d[4]_{7/2} - 6p[3]_{5/2}$ spin split electronic transition of Xe II at 834.72 nm is relatively narrow at approximately 500 MHz and the line structure can be neglected to a large degree in analysis of Hall effect thruster plasma dynamics.[22,23] However, the Xe I $6s[3/2]^0_2 - 6p[3/2]_2$ transition at 823.18 nm is dramatically broader and visually more complex due to the spin split odd isotopes.[12] Furthermore as the mass of the atoms of interest is lowered, the energy separation between the various isotope's transitions increases as the fractional changes in nuclear mass increase. As a result, knowledge of these isotope constants becomes increasingly important important to adequately interpret the fluorescence spectra.

Neutral Krypton

A survey of the available literature shows that there is limited, but adequate, available data on the isotope and hyperfine spin splitting constants for Kr I. The available literature is sufficient to examine a number of potential transitions as candidates for investigations of the neutral dynamics in a Kr Hall effect thruster and a number of transition appear suitable for diagnostics development.

A cursory examination of the literature shows that there is a dichotomy in the available data. Especially

for neutral krypton, there are a number of transitions for which the ^{83}Kr nuclear spin splitting is available, but the isotope shifts are not readily available. This appears to be due to the interest in the physics community to understanding nuclear structure.

The present availability Kr I hyperfine splitting data is best summarized by Cannon and Janik.[24] This work examines eight transitions from from the $5s'[1/2]_\circ$ and $5s[3/2]_2$ metastable energy states. Of the transitions presented, two Kr I transitions appear to be strong candidates, the $5s[3/2]_2$–$5p[5/2]_2$ at 810.44 nm and $5s[3/2]_2$–$5p[3/2]_2$ at 760.15 nm. Several other transitions are also sufficiently well characterized, but fitting with our previous criteria we have chosen to remain in the regime where presently available tunable diode lasers can operate. For example, a well characterized neutral transition exists at 556 nm which is probably better suited for dye laser interogration.[25]

The Kr I $5s[3/2]_2$–$5p[5/2]_2$ transition at 810.44 nm appears to be a reasonable choice for further study. The fluorescence decay from the $5p[5/2]_2$ can take any of 3 transitions and from examination of the limited Einstein coefficients for spontaneous emission the transition at 877.6 nm will have have an approximate branching ratio of 65% and the resonant fluorescence will have a branching ratio of approximately 30%.[26]

The Kr I $5s[3/2]_2$–$5p[5/2]_2$ transition at 810.44 nm also has one other very interesting characteristic. The upper $5p[5/2]_2$ state is only 1.6×10^{-3} eV above the $5p[5/2]_3$ state.[26] While this does not affect the requirements for use of this transition for the aforementioned purposes of characterization of the neutral flow velocity, the proximity of this state to the upper state of the $5s[3/2]_2$–$5p[5/2]_2$ transition at 810.44 nm does open up some interesting diagnostic possibilities. Previous work in higher density plasmas has used collisional transfer of laser excited states to nearby states and followed the subsequent fluorescence from these collisional connected states to determine collision rates and electron temperatures and densities.[27] This diagnostic technique is known as laser-collision induced fluorescence (LCIF) and is defined as the emission of states populated by laser excitation and a subsequent collision. It appears that further effort could develop a similar diagnostic technique for krypton plasmas with this, and perhaps other, transitions. Obviously, more study of the collisional probabilities of these states would be required to develop this capability.

The Kr I $5s[3/2]_2^\circ$–$5p[3/2]_2$ at 760.15 nm has been studied more extensively and exhibits some properties that make it our choice for further study.[24] Young, et al.,[28] also extensively examined the mechanics of this transition. The lower $5s[3/2]_2^\circ$ state is metastable with a measured lifetime of approximately 40 s. The decay branching ratio from the upper $5p[3/2]_2$ state is 77% to the $5s[3/2]_2^\circ$ state making this transition a very efficient transition for examination of resonant fluorescence.

Table 3 Isotope Shifts for the Kr I $5s[3/2]_2^\circ$–$5p[3/2]_2$ transition at 760.15 nm[24]

Isotope	Isotope Shift MHz
78	233.56
80	147.99
82	69.311
83	20.704
84	0
86	-73.411

Table 4 Spin Splitting Constants for the ^{83}Kr I $5s[3/2]_2^\circ$–$5p[3/2]_2$ transition at 760.15 nm[24]

Electronic State	A Coefficient MHz	B Coefficient MHz
$5s[3/2]_2^\circ$	-243.934	-452.936
$5p[3/2]_2$	-108.611	-88.615

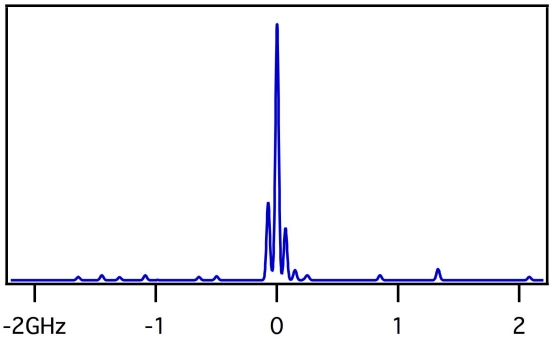

Fig. 1 Cold spectrum (1 K) of $5s[3/2]_2^\circ$–$5p[3/2]_2$ transition at 760.15 nm.

Cannon and Janik have measured the spin splitting of the ^{83}Kr as well as the isotope shifts of the even isotopes[24] as summarized in Tables 3 and 4. These data allow for us to simulate the line shape for a number of conditions.

Figure 1 shows cold spectrum (1 K) of the $5s[3/2]_2^\circ$–$5p[3/2]_2$ transition at 760.15 nm where the natural line width has been neglected.[5] The general structure of the composite transition is a cluster of the 5 even isotopes surrounded by the 13 spin split transitions due to ^{83}Kr. As a result, the majority of the structure is determined by the even isotope separation. For the remainder of the analysis, we will continue to neglect the natural lineshape as well as collisional broadening contributions to the total lineshape. We preliminarily judge this as suitable for the study of the relatively high mass of Kr.

Figure 2 shows the transition line shape at a much

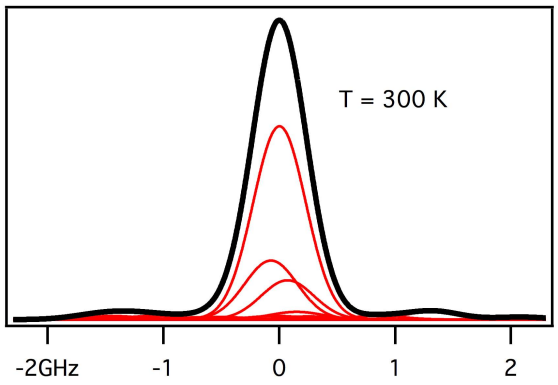

Fig. 2 300 K spectrum of $5s[3/2]^\circ_2$–$5p[3/2]_2$ Kr I transition at 760.15 nm showing the contributions of the 18 individual components.

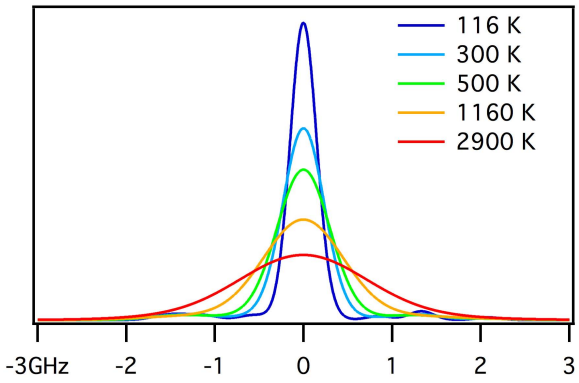

Fig. 3 Multitemperature spectrum of $5s[3/2]^\circ_2$–$5p[3/2]_2$ Kr I transition at 760.15 nm.

more likely to be observed temperature of 300 K. The core of the composite lineshape is determined by the cluster of even isotopes. The relatively low fraction of ^{83}Kr (11.55%) results in the spin split transitions contributing relatively little to the overall structure. As shown in Fig. 2, the spin split components contribute to the presence of outlying hyperfine line shape structure ±1.5 GHz from the line center; however as shown in Fig. 3, the low magnitude of the spin split components makes the outlying structure relatively small and lessen with increased Doppler broadening (temperature).

Examining the structure of the line shapes in Fig. 3 in more detail, it is interesting to note that the cumulative full width at half maximum (FWHM) is only slightly higher than the Doppler width of a single component as shown in Fig. 4. This can can be readily attributed to three factors. The effect of the ^{83}Kr spin split components is limited to their large number (13) and spacing. Furthermore, the relatively limited fraction of naturally occurring ^{83}Kr (11.55%) limits the

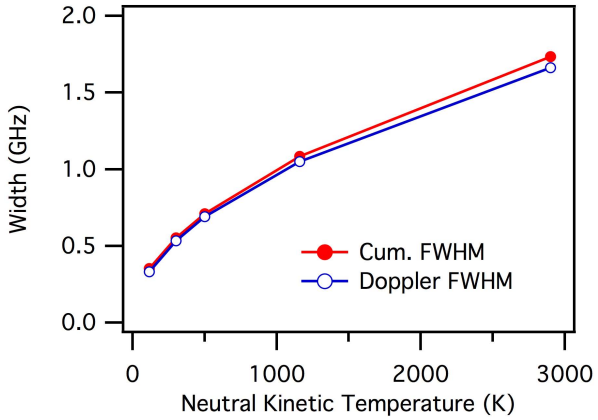

Fig. 4 Cumulative line width (FWHM) and Doppler line width compared for the Kr I $5s[3/2]^\circ_2$–$5p[3/2]_2$ transition at 760.15 nm.

cumulative effect of the spin split components. Finally, the even isotope shifts are in general relatively small as shown in Table 3. Therefore, the composite lineshape is relatively narrow.

Singly Ionized Krypton

The most recent review of Kr II transitions suitable for diagnostics of plasma thrusters is by Scharfe.[15] His survey of available transitions has identified only a single transition where both the isotope and spin split hyperfine constants are known. The Kr II $5d^4D_{7/2}$–$5p^4P^\circ_{5/2}$ transition at 728.98 nm has received the most study of the several lines identified by Scharfe.

Scholl, et al.[29] measured the lower $5d^4D_{7/2}$ state A and B spin splitting constants for ^{83}Kr to high accuracy as shown in Table 5. While Schuessler et al.[30] measured the spin splitting constants for the upper $5p^4P^\circ_{5/2}$ state also shown in Table 5. Schuessler et al. also measured the isotope shifts of the 728.98 nm $5d^4D_{7/2}$–$5p^4P^\circ_{5/2}$ transition as shown in Table 6. From our research as well as that performed by Scharfe, it appears that this is the only Kr II transition for which the hyperfine structure has been fully characterized.

From the $5p^4P^\circ_{5/2}$ state the there are 6 known transitions for the fluorescence decay. Using available Einstein coefficients for spontaneous emission, there appears to be a transition, $5s^4P_{5/2}$–$5p^4P^\circ_{5/2}$, at 473.90 nm with a greater than 80% branching ratio.[26] The resonant fluorescence for the $5d^4D_{7/2}$–$5p^4P^\circ_{5/2}$ transition appears to be approximately 10%, but due to incomplete knowledge of the relevant coefficients for spontaneous emission,is likely lower.

Using the information in Tables 5 and 6, the line structure of the 728.98 nm $5d^4D_{7/2}$–$5p^4P^\circ_{5/2}$ transition may be modeled. Again, we assume Doppler broadening to be the the only significant mechanism in this preliminary analysis.

Figure 5 shows the cold (1 K) transition. As in the case of the neutral transition, the higher peaks

Table 5 Spin Splitting Constants for the ^{83}Kr II $5d^4D_{7/2}$–$5p^4P^\circ_{5/2}$ transition at 728.98 nm[29,30]

Electronic State	A Coefficient MHz	B Coefficient MHz
$5d^4D_{7/2}$	-43.513	-294.921
$5p^4P^\circ_{5/2}$	-167.2	+91

Table 6 Isotope Shifts for the Kr II $5d^4D_{7/2}$–$5p^4P^\circ_{5/2}$ transition at 728.98 nm[30]

Isotope	Isotope Shift MHz
78	1185.7
80	768.0
82	372.6
83	175.0
84	0
86	-365.2

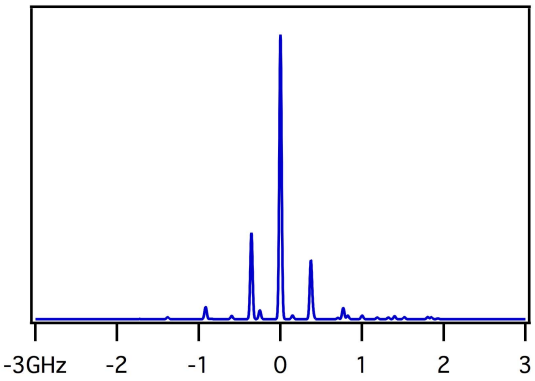

Fig. 5 Cold spectrum (1 K) of the Kr II 728.98 nm $5d^4D_{7/2}$–$5p^4P^\circ_{5/2}$ transition.

represent the even isotopes while the more outlying, lower magnitude peaks are due to the spin split ^{83}Kr isotope.

Figure 6 shows the line shape for a variety of temperatures, up to 2900 K, or 0.25 eV. Temperatures above 0.25 eV do not exhibit any visible structure. This upper limit was chosen based on previous measurements which showed that the ion temperatures, as near as they can be defined, are low as measured in radial measurements.[6] In fact, the line shape in the axial direction actually appears to be dominated by discharge plasma dynamics and these are reflected in the axial fluorescence line shape.[23]

It is interesting to note that the isotope shifts are significantly larger for this transition than the neutral transition previously examined. As a result, Fig. 6 shows a clear broadening of the line cumulative width

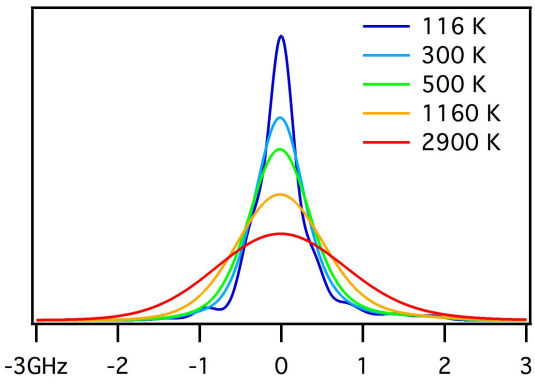

Fig. 6 Multitemperature spectrum of the Kr II 728.98 nm $5d^4D_{7/2}$–$5p^4P^\circ_{5/2}$ transition.

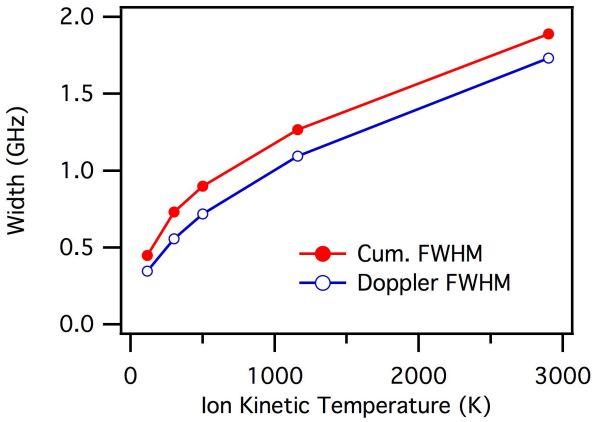

Fig. 7 Cumulative line width (FWHM) and Doppler line width compared for the Kr II 728.98 nm $5d^4D_{7/2}$–$5p^4P^\circ_{5/2}$ transition.

relative to a single component Doppler width due to the isotope shifts. The difference appears to be a consistent 200 MHz. The difference appears to be nearly constant in the range examined.

Future Work

We have selected the Kr II $5d^4D_{7/2}$–$5p^4P^\circ_{5/2}$ transition at 728.98 nm ($\Delta E = 13,713.989$ cm^{-1}) to continue our initial investigation of krypton fueled Hall effect thrusters. We have purchased and taken delivery of a custom built ±50 GHz tunable diode laser (Newport Optics, New Focus Division) centered on the $5d^4D_{7/2}$–$5p^4P^\circ_{5/2}$ transition with a minimum of 10 mW output power.

The krypton Hall thruster will be mounted on a three axis orthogonal translation system. As envisioned and based on previous efforts,[31] produced, the diode laser beam will be passed through a Faraday isolator to eliminate laser feedback. The beam then will pass through a number of beam pick-offs (BS) until focused by a lens and enter the vacuum chamber

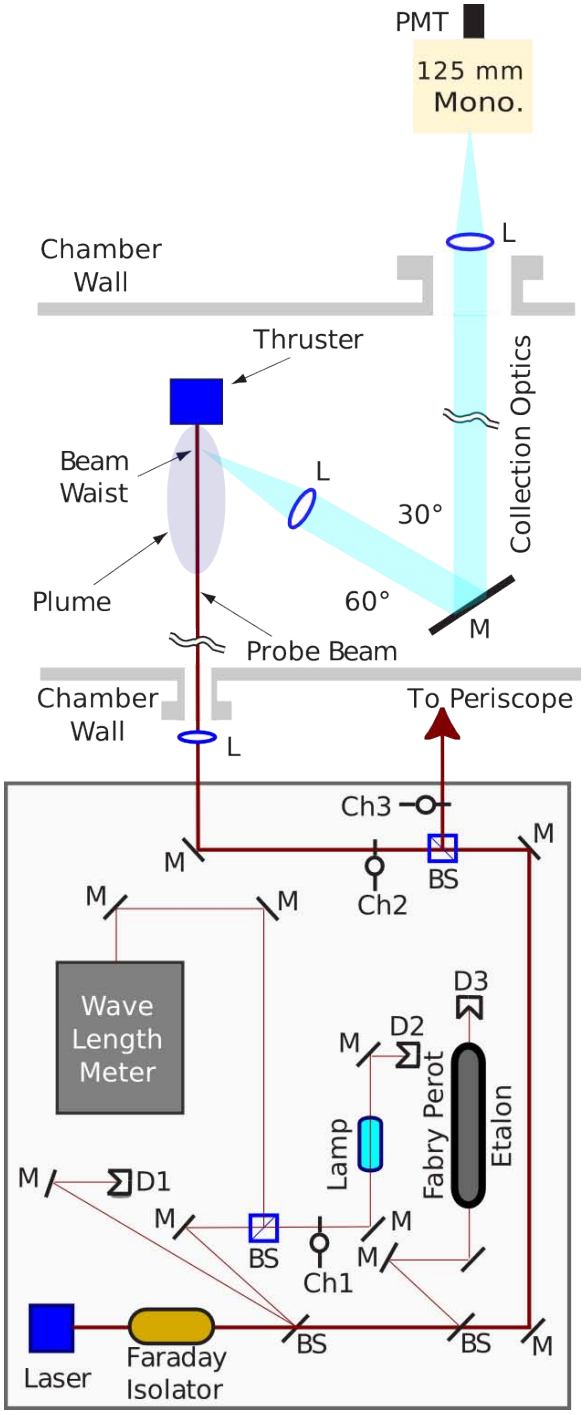

Fig. 8 Typical layout of a LIF apparatus suitable for interrogation of a Hall thruster or other electric propulsion thruster.[31]

through a window. The probe beam will be chopped at kHz frequencies by an optical chopper for phase sensitive detection.

The two wedge beam pick-offs (BS) shown in Fig. 8 will provide beam diagnostics. The first beam pick-off will direct a beam to a photodiode detector (D1) used to provide constant power feedback to the laser. The second beam will be divided into two equal components by a 50-50 cube beam splitter (BS). The first component will be directed to a commercial wavelength meter used to monitor absolute wavelength. The second component will be sent through another optical chopper and through a reference lamp or cell.

The type of absolute wavelength reference to be used has not yet been definitively selected. Most discharge lamps will not produce a sufficient population of metastable ions to serve as a suitable reference. We have tentatively chosen to examine two options. First, a low pressure krypton resonant microwave discharge cavity should be sufficiently energetic to produce a suitable population of metastable ions to serve as a absorption cell for the the Kr II $5d^4D_{7/2}$–$5p^4P^{\circ}_{5/2}$ transition at 728.98 nm. We have some concerns due to electronic noise and potential of microwave leakage to damage instrumentation. Although use of the Kr II absorption spectrum directly is appealing, we are also alternatively considering the use of a heated iodine cell. Iodine has a rich and well mapped rotational–vibrational molecular spectrum that is commonly used as wavelength markers in the visible and into the red portion of the spectrum. At 728.98 nm, suitable rotational–vibrational absorption spectra are available provided the cell is heated to several hundred °C. The option of using a nearby absorption feature from a glow discharge lamp does not appear to be available to us in this wavelength range.[26]

The second pick-off will send a beam to a 300 MHz free spectral range Fabry-Perot etalon (F-P) that provides high resolution frequency monitoring of the wavelength interval swept during a laser scan.

The fluorescence collection optics are also shown in Fig. 8. The fluorescence will be collected by a 75 mm diameter, 300 mm focal length lens within the chamber. The collimated signal will be directed through a window in the chamber side wall to a similar lens that will focus the collected fluorescence onto the entrance slit of 125 mm focal length monochrometer with a photomultiplier tube (PMT). The spatial resolution of the measurements will of course be determined by the geometry of the spectrometer entrance slit (recall 1:1 magnification of the collection optics).

Conclusions

We have presented the background research to measure the flow fields of a krypton plasma thruster using LIF. We have selected suitable spectral lines for both Kr I and Kr II and created models for their analysis. Although preliminary, we believe that these analyses are sufficient to proceed with the development of an experimental apparatus.

The development of krypton specific laser diagnostics for plasma thrusters, especially Hall effect thrusters appears to have justification due to large price fluctuations for xenon as well as limited production. In some cases, especially orbit maintenance,

the use of krypton fuels may offer distinct advantages due to its lower atomic mass producing a 25% increase in exit velocity. This must of course be tempered by the larger propellant tankage fraction likely required to store an equal mass of krypton versus xenon.

There is also some sound science in development of these krypton LIF diagnostics. Optically probing the interiors of plasma thrusters such as the Hall effect thruster is in its infancy. The study of multiple species has before increased the understanding of charged particle generation and transport within these devices.[32] Those early studies were of course limited to electrostatic probe measurements and did not have the benefit of nonintrusive measurements of velocities, velocity distributions, and in some cases temperatures.

Another issue that bears greater examination is the possible diagnostic development of Kr I $5s[3/2]_2$–$5p[5/2]_2$ transition at 810.44 nm for LCIF. Should this transition be suitable, it would provide a diagnostic capable of measuring at least the relative electron–neutral collision frequency. If two suitable nearby transitions can be identified and specific electron-neutral collisional cross–sections can be measured or estimated, it may be possible to measure the electron density and temperature simultaneously. Since this technique would require saturation of the pumped transition, the use of higher power pulsed lasers would also lend itself to the development of phase synchronized data analysis to measure plasma periodic behavior.

Acknowledgments

The author would like to thank a number of fruitful discussions that enabled this paper. This includes early discussions with Drs. M. Cappelli and D. Scharfe at Stanford University, and Dr. Gascon from Space Systems Loral. The author also acknowledges Dr. K. Polzin for encouragement that ensured the completion of this paper. The author also wishes to thank Ms. N. MacDonald of AFRL for her assistance in the presentation of this paper. Finally, the paper would not have been written except for the strong encouragement received early from Dr. C. Larson who would have found this effort to be *a good start.*

References

[1]Jahn, R., *Physics of Electric Propulsion*, McGraw-Hill, 1968.

[2]Lide, D. R., *Handbook of Chemistry and Physics*, CRC Press, 79th ed., 1998.

[3]Duchemin, O., Valentian, D., and Cornu, N., "Cryostorage of Propellants for Electric Propulsion," *Proceedings of the 45th Joint Propulsion Conference and Exhibit*, No. AIAA-2009-4912, American Institute of Aeronautics and Astronautics, August 2009.

[4]Ecckbreth, A. C., *Laser Diagnostics For Combustion Tempterature and Species*, Gordon and Breach Publishers, 1988.

[5]Demtroder, W., *Laser Spectroscopy: Basic Concepts and Instrumentation*, Springer-Verlag, 1996.

[6]Hargus Jr., W. A. and Cappelli, M. A., "Laser-Induced Fluorescence Measurements of Velocity within a Hall Discharge," *Applied Physics B*, Vol. 72, No. 8, June 2001, pp. 961–969.

[7]Hargus, W. A. and Charles, C. S., "Near Exit Plane Velocity Field of a 200 W Hall Thruster," *Journal of Propulsion and Power*, Vol. 24, No. 1, January-February 2008, pp. 127–133.

[8]Mazouffre, S., Gawron, D., Kulaev, V., and Sadeghi, N., "A laser spectroscopic study on Xe+ ion transport phenomena in a 5 kW-class Hall effect thruster," *Proceedings of the 30th International Electric Propulsion Conference*, No. IEPC-2007-160, Electric Rocket Society, Florence, Italy, September 2007.

[9]Nakles, M. R. and Hargus Jr., W. A., "Background Pressure Effects on Internal and Near-field Ion Velocity Distribution of the BHT-600 Hall Thruster," *Proceedings of the 44th Joint Propulsion Conference and Exhibit*, No. AIAA-2008-5101, American Institute of Aeronautics and Astronautics, Hartford, CT, July 2008.

[10]Hargus Jr., W. A., Nakles, M. R., Pote, B., and Tedrake, R., "The Effect of Thruster Oscillations on Axial Velocity Distributions," *Proceedings of the 44th Joint Propulsion Conference and Exhibit*, No. AIAA-2008-4724, American Institute of Aeronautics and Astronautics, Hartford, CT, July 2008.

[11]Fujimoto, T. and Iwamae, A., editors, *Plasma Polarization Spectroscopy*, Vol. 44 of *Series on Atomic, Optical and Plasma Physics*, Springer-Verlag, 2008.

[12]Cedolin, R., *Laser-Induced Fluorescence Diagnostics of Xenon Plasmas*, Ph.D. thesis, Stanford University, June 1997.

[13]Manzella, D. H., "Stationary Plasma Thruster Ion Velocity Distribution," *Proceedings of the 30th Joint Propulsion Conference and Exhibit*, No. AIAA-1994-3141, American Institute of Aeronautics and Astronautics, June 1994.

[14]Hargus Jr., W. A. and Nakles, M. R., "Ion Velocity Measurements within the Acceleration Channel of Low Power Hall Thruster," *Proceedings of the 30th International Electric Propulsion Conference*, No. IEPC-2007-172, Electric Rocket Society, Florence, Italy, September 2007.

[15]Scharfe, D. B., *Alternative Hall Thruster Propellants Krypton and Bismuth: Simulated Performance and Characterization*, Ph.D. thesis, Stanford University, Palo Alto, CA, August 2009.

[16]Hargus Jr., W. A., "Laser-Induced Fluorescence Measurements of Neutral Xenonin the Near Field of a 200 W Hall Thruster," *Proceedings of the 41st Joint Propulsion Conference and Exhibit*, No. AIAA-2005-4400, American Institute of Aeronautics and Astronautics, Tucson, AZ, July 2005.

[17]Cannon, B. D. and Whitaker, T. J., "A New Laser Concept for Isotopically Selective Analysis of Noble Gases," *Applied Physics B*, Vol. 38, No. 1, September 1985, pp. 57–64.

[18]Trickl, T., Vrakking, M. J. . J., Cromwell, R., Lee, Y. T., and Kung, A. H., "Ultrahigh-Resolution (1+1) Photoionizaiton Spectroscopy of Kr I: Hyperfine Structures, Isotope Shifts, and Lifetimes for the n = 5, 6, 7 4p5 ns Rydberg Levels," *Phyiscal Review A*, Vol. 39, No. 6, 1 March 1989, pp. 2948–2955.

[19]Cowan, R. D., *The Theory of Atomic Structure and Spectra*, University of California Press, Berkeley, CA, 1981.

[20]Sobelman, I. I., *Atomic Spectra and Radiative Transitions*, Springer-Verlag, Berlin, 1992.

[21]White, H. E., *Introduction to Atomic Spectra*, McGraw-Hill, New York, 1934.

[22]Hargus, W. A. and Charles, C. S., "Near-Plume Laser-Induced Fluorescence Velocity measurements of a Medium Power Hall Thruster," *Journal of Propulsion and Power*, Vol. 26, No. 1, January-February 2010, pp. 135–141.

[23]Hargus Jr., W. A. and Nakles, M. R., "Evolution of the Ion Velocity Distribution in the Near Field of the BHT-200-X3 Hall Thruster," *Proceedings of the 42nd Joint Propulsion Conference and Exhibit*, No. AIAA-2006-4991, American Institute of Aeronautics and Astronautics, Sacramento, CA, July 2006.

[24]Cannon, B. D. and Janik, G. R., "Hyperfine Splittings and Isotope Shifts in Eight Transitions from the Metastable 4p5 5s

J=2 and J=0 states of Kr I," *Phyiscal Review A*, Vol. 42, No. 1, 1 July 1990, pp. 397–402.

[25]Champeau, R. J. and Keller, J. C., "Spectroscopie Laser a Tres Haute Resolution Sur un Jet Atomique de Krypton," *Journal of Phyiscs B*, Vol. 11, No. 3, 1978, pp. 391–397.

[26]Ralachenko, Y., Kramida, A. E., Reader, J., and Team, . N. A., "NIST Atomic Spectra Data Base Version 3.1.5," Tech. rep., National Institute of Standards and Technology, Gaithersburg, MD, July 2010.

[27]Dzierzega, K., K, M., E, C, B., and Roberts, J. R., "Electron Density Measurement in a RF Helium Plasma by Laser-Collision Induced Fluorescence," *Journal of Applied Physics*, Vol. 80, No. 6, 15 September 1996, pp. 3196–3201.

[28]Young, L., Yang, D., and Dunford, R. W., "Opitical Production of Metastable Krypton," *Journal of Phyiscs B*, Vol. 35, 2002, pp. 2985–2992.

[29]Scholl, T. J., Gaily, T. D., Holt, R. A., and Rosner, S. D., "Fast-Ion-Beam Laser and Laser-RF Double Resonance Measurements of Hyperfine Structure in 83Kr II," *Phyiscal Review A*, Vol. 33, No. 4, April 1986, pp. 2396–2400.

[30]Schuessler, H. A., Alousi, A., Idrees, M., Li, Y. F., Buchinger, F., Evans, R. M., and Fischer, C. F., "Isotope Shifts and Hyperfine-Structure-Splitting Constants of the 4d-5p transition in Kr II at 729 nm," *Phyiscal Review A*, Vol. 45, No. 9, 1 May 1992, pp. 6459–6467.

[31]Hargus, W. A. and Nakles, M. R., "Ion Velocity Measurements within the Acceleration Channel of Low-Power Hall Thruster," *IEEE Transactions on Plasma Science*, Vol. 36, No. 5, October 2008, pp. 1989–1997.

[32]Janes, G. S. and Lowder, R. S., "Anomalous Electron and Ion Acceleration in a Low-Density Plasma," *Physics of Fluids*, Vol. 6, 1966, pp. 1115.